Kink in the Dispersion of Layered Strontium Ruthenates

Y. Aiura,[1,*] Y. Yoshida,[1,2] I. Hase,[1] S. I. Ikeda,[1] M. Higashiguchi,[3] X. Y. Cui,[3] K. Shimada,[4] H. Namatame,[4] M. Taniguchi,[3,4] and H. Bando[1]

[1]*National Institute of Advanced Industrial Science and Technology, Tsukuba, Ibaraki 305-8568, Japan*
[2]*Japan Society for the Promotion of Science, Chiyoda, Tokyo 102-8471, Japan*
[3]*Graduate School of Science, Hiroshima University, Higashi-Hiroshima 739-8526, Japan*
[4]*Hiroshima Synchrotron Radiation Center, Hiroshima University, Higashi-Hiroshima 739-8526, Japan*

(Received 13 April 2004; published 10 September 2004)

We present detailed energy dispersions near the Fermi level along the high symmetry line ΓX on the monolayer and bilayer strontium ruthenates Sr_2RuO_4 and $Sr_3Ru_2O_7$, determined by high-resolution angle-resolved photoemission spectroscopy. A kink in the dispersion is clearly shown for the both ruthenates. The energy position of the kink and the slope in the low-energy part near the Fermi level are almost identical between them, whereas the dispersion in the high-energy part varies, like the behavior of the kink for the cuprate superconductors.

DOI: 10.1103/PhysRevLett.93.117005 PACS numbers: 74.70.Pq, 74.25.Jb, 79.60.–i

The Ruddlesden-Popper (RP)-type ruthenates $(Sr, Ca)_{n+1}Ru_nO_{3n+1}$ with perovskite-based crystal structure have attracted significant attention in solid-state physics since superconductivity was discovered in the layered material Sr_2RuO_4 ($n = 1$) at $T_c = 1.5$ K [1–3]. From recent angle-resolved photoemission spectroscopy (ARPES) studies of Sr_2RuO_4 [4,5], it was shown that the experimental Fermi surface topology determined by ARPES is fairly consistent with the de Haas–van Alphen results [6] and the calculated band structure [7]. The most three dimensional (3D) $SrRuO_3$ ($n = \infty$) is an itinerant ferromagnetic (FM) metal [8]. The bilayer perovskite $Sr_3Ru_2O_7$ ($n = 2$) is regarded as having an intermediate dimensionality between the systems with $n = 1$ and $n = \infty$ [9]. The Fermi liquid behavior and FM instability in the ground state were shown [10,11] and metamagnetism was confirmed by transport and magnetization measurements [12,13]. From a viewpoint of the electronic structure, the crucial difference between the monolayer and bilayer systems is the existence of an intracell interaction between the RuO_2 layers.

In the previous ARPES studies on the bilayer system $Sr_3Ru_2O_7$, it was shown that the bilayer coupling in the electronic structure leads only to a slight splitting of the band centered at the Γ point and the experimental Fermi surface is closely related to that of the monolayer system Sr_2RuO_4 [14,15]. The ARPES results remarkably contradict the theoretical prediction from the band calculation [16,17]. Recently, the role of the bilayer coupling in the electronic structure has been extensively discussed for the cuprate high-temperature superconductors [18,19]. Since the conduction band is derived from an in-plane Cu $3d_{x^2-y^2}$ hole, the magnitude of the splitting is not so large (less than 100 meV). On the other hand, the conduction bands for the RP-type ruthenates are derived from not only an in-plane Ru $4d_{xy}$ electron but also two out-of-plane Ru $4d_{yz,zx}$ electrons. Therefore, the electronic structure for the bilayer system $Sr_3Ru_2O_7$ may be drastically rearranged due to the large bilayer coupling of the out-of-plane Ru $4d_{yz,zx}$ electrons.

In this Letter, we present detailed band dispersions along the high symmetry line ΓX of the monolayer and bilayer systems, Sr_2RuO_4 and $Sr_3Ru_2O_7$, determined by high-resolution ARPES. A kink in the dispersion is clearly shown for both systems. Although there is a strong bilayer coupling in $Sr_3Ru_2O_7$, the energy position of the kink and the slope in the low-energy part near the Fermi level (E_F) is almost the same between them, whereas the dispersion in the high-energy part varies, which is similar to the behavior of the kink shown for the cuprate superconductors [20].

For single crystal growth by a floating zone (FZ) method, we employed a self-flux technique. Details of the FZ crystal growth are explained elsewhere [10,11]. In order to obtain clean surfaces, we cleaved the single crystalline samples $Sr_3Ru_2O_7$ *in situ* in ultrahigh vacuum (below 1×10^{-10} Torr) at 10 K, whereas we cleaved Sr_2RuO_4 at 160 K to prevent the rotation of the RuO_6 octahedron at the surface [5,21]. The present measurements were carried out on a high-resolution linear undulator beam line (BL-1) connected to the compact electron-storage ring (HiSOR) located at Hiroshima Synchrotron Radiation Center (HSRC), Hiroshima University [22,23]. The radiation is linearly polarized in the horizontal plane of incidence. The beam line is equipped with a high-resolution, hemispherical electron analyzer (SCIENTA ESCA200). With the setup, it is possible to simultaneously measure multiple energy distribution curves in an angular window of 11° horizontally. The angular resolution was 0.5° (vertical) ×0.3° (horizontal). All ARPES spectra were taken along a high symmetry line ΓX at a photon energy ($h\nu$) of 27 eV and a temperature of 10 K. Then, the spatial resolution of the angular window (0.3°) corresponds to a k resolution of 1.1% of the ΓX line. The total instrumental energy resolution was set at 20 meV, which was confirmed by the

photoemission spectra of the Fermi edge of evaporated Au. The samples were mounted vertically and only photoelectrons emitted from the plane defined by the light beam and the surface normal were observed. The emission angle of the photoelectron measured from the surface normal was varied around the vertical axis. In the configuration, the radiation is polarized in the detection plane (p polarization). Then, a nonvanishing photoemission matrix element implies that the initial-state wave functions must be symmetric with respect to the detection plane if we take ARPES spectra along the high symmetry line [24]. Recently, significant matrix element effects of the polarized light were shown for some quasi-two-dimensional (quasi-2D) materials [25].

Before discussing the ARPES spectra, we consider the band structure along the ΓX line in detail. In previous ARPES studies on $h\nu$ dependence of the valence band of $Sr_3Ru_2O_7$ [14], the spectral features appear to be without dispersion as a function of $h\nu$, suggesting the 2D nature of the electronic states. Band calculations also showed a strong 2D character in the electronic structure of Sr_2RuO_4 [7,26–28] and $Sr_3Ru_2O_7$ [16,17]. Therefore, we omitted the slight energy dispersion along the k_z direction and compared all ARPES spectra with the calculated band dispersion along the ΓX line. In addition, we ignored the effects of the orthorhombic distortion of $Sr_3Ru_2O_7$ in the band calculation [16] because the influence of the distortion on the ARPES spectra is faint as discussed later.

Figure 1(a) shows the calculated bands crossing E_F of Sr_2RuO_4 [28], and Fig. 1(b) $Sr_3Ru_2O_7$ [16] along the ΓX line. For the monolayer system Sr_2RuO_4, there are three bands crossing E_F, which compose three Fermi surfaces [4,6]. The Δ_1 band is caused by the Ru $4d_{xy}$ orbital, whereas the Δ_2 and Δ_4 bands, which degenerate at the Γ point, by the admixture of Ru $4d_{yz}$ and $4d_{zx}$ orbitals [29]. For the bilayer system $Sr_3Ru_2O_7$, there are six bands crossing E_F. A pair of bands with Δ_1 and Δ_4 symmetry appears from the Δ_1 band derived from the Ru $4d_{xy}$ oribital in the monolayer system. Similarly, the Δ_4 band (Ru $4d_{yz,zx}$) in the monolayer system also is split into Δ_1 and Δ_4 bands in the bilayer system. Since two bands with the same symmetry in the bilayer system are coupled with each other, those bands are caused by the in-plane Ru $4d_{xy}$ and out-of-plane $4d_{yz,zx}$ orbitals. On the other hand, the Δ_2 band in the monolayer system is split into a pair of bands with Δ_2 and Δ_3 symmetry, which do not contain the contribution from in-plane Ru $4d_{xy}$ orbital (broken lines in Fig. 1(b)]. As shown in the energy splitting at the Γ point in Fig. 1(b), it is well known that the bilayer coupling between the out-of-plane Ru $4d_{yz,zx}$ orbitals ($\Delta E_{yz,zx}$) is large compared with that between the in-plane Ru $4d_{xy}$ orbital (ΔE_{xy}).

Figures 2(a) and 2(b) show momentum distribution curves (MDC's) spaced by 5 meV of $Sr_3Ru_2O_7$ along the ΓX line and the intensity plot, respectively. At first sight, it is well known that three prominent spectral features,

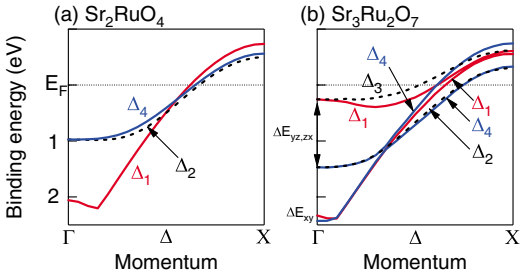

FIG. 1 (color online). The calculated energy bands crossing E_F for the tetragonal structure of (a) Sr_2RuO_4 [28] and (b) $Sr_3Ru_2O_7$ [16] along the high symmetry line ΓX.

denoted by A, B, and C, disperse upward in energy with increasing the momentum. In the MDC's near E_F, the spectral width of feature B is very broad compared with that of feature A, as shown in Figs. 2(a) and 4(b). Figure 2(c) shows the experimental band dispersion, which is extracted by fitting the MDC's with three Lorentzian functions plus a small k-independent background, together with the calculated band structure in Fig. 1(b). The spectral feature B becomes obscure with an increasing binding energy, and it is hard to estimate the peak position correctly above the binding energy of 30 meV. Comparing the experimental band dispersion with the calculated one, one may suppose that the sharp spectral feature A is derived from the Δ_2 and Δ_4 bands, the broad spectral feature B from two Δ_1 and Δ_4 bands, and the remaining spectra feature C from the Δ_3 band. However, we should recall the matrix element effects for the ARPES spectra as described above. The Δ_1 and Δ_4 bands as shown by the solid curves in Fig. 2(c) are symmetric with respect to the detection (mirror) plane, whereas the Δ_2 and Δ_3 bands (the broken curves) are antisymmetric. Since we performed the ARPES experiments using the p-polarized light, the Δ_2 and Δ_3 bands

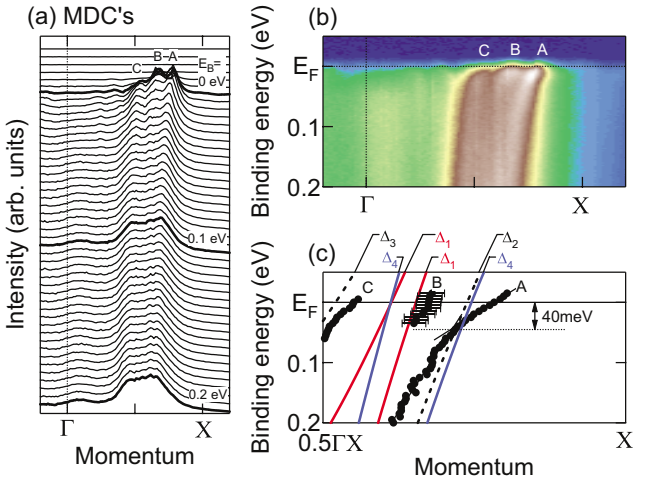

FIG. 2 (color online). (a) MDC's, (b) intensity plot, and (c) experimental band dispersion relation of $Sr_3Ru_2O_7$ along the high symmetry line ΓX.

become optically forbidden in the configuration. Based on the matrix element effects, it is considered that spectral feature A, which is sharper than spectral feature B, may be mainly derived from the Δ_4 band. Similarly, it is possible that spectral feature C is derived from the Δ_4 band on the left-hand side or the Δ_1 band on the left-hand side because the Δ_3 band is optically forbidden. Otherwise, the Δ_3 band may be partially shown if the matrix element effects are imperfect due to the spin-orbit interaction [30] and/or the k_z of the electronic structure. There is room for further investigation about the detailed assignment.

Next, Fig. 2 indicates a kink in the dispersion of spectral feature A around 40 meV, as reported in ARPES spectra of the cuprate superconductors [20,31]. To investigate the existence of a similar kink structure for the monolayer system Sr_2RuO_4, we have taken ARPES spectra along the same line. Figure 3(a) shows MDC's, and Fig. 3(b) the intensity plot along the ΓX line. The MDC-derived dispersions are shown by solid circles in Fig. 3(c) together with the calculated band structure. In the MDC at E_F in Fig. 3(a), two spectral features are shown. The prominent feature on the right-hand side is mainly derived from the Δ_4 band, which makes the γ Fermi surface [32]. The other feature is derived from the Δ_1 band, which makes the β Fermi surface. From the experimental dispersion in Figs. 3(b) and 3(c), a similar kink structure is clearly shown for the Δ_4 band of Sr_2RuO_4. From the kink structure, the effective band mass of the Δ_4 band, or the γ Fermi surface, is enhanced near E_F, which is qualitatively consistent with that in previous studies of magneto-oscillatory phenomena and specific heat [6,33]. To compare the behavior of the kink between the monolayer and bilayer systems in detail, the experimental dispersion of spectral feature A of $Sr_3Ru_2O_7$ is shown by the open circles in Fig. 3(c), where the Fermi momentum is arranged at that of Sr_2RuO_4. As shown in the Fig. 3(c), the energy position of the kink (at about 40 meV) and the slope in the low-energy part near E_F is almost the same between the monolayer and bilayer systems, whereas the dispersion in the high-energy part varies between them. The universality of the slope in dispersion, or Fermi velocity, shown here is also shown for the cuprate [20], but the mechanism remains an unsettled question.

The interpretation of the kink structure for the cuprates has been controversial. In recent works, it was related to phonons [31,34,35] or magnetic excitations [36–39]. The kink of the layered ruthenates was observed well above T_c, that is, in the normal state, whereas the magnetic excitations of the cuprates set in T_c. In addition, the magnetic ground state is different in the monolayer and bilayer strontium ruthenates, Sr_2RuO_4 and $Sr_3Ru_2O_7$ [10], but the spectral behavior of the kinks in Figs. 2 and 3 are similar as well. Therefore, it may be hard to simply ascribe the kink for the layered ruthenates to the magnetic excitations. On the other hand, little information is available at the moment about high-energy phonons,

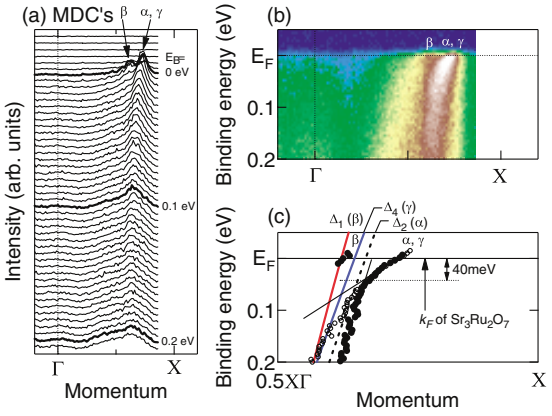

FIG. 3 (color online). (a) MDC's and (b) intensity plot of Sr_2RuO_4 along the high symmetry line ΓX. (c) The MDC-derived dispersions (solid circles) together with the calculated band structure. The dispersion of spectral feature A of $Sr_3Ru_2O_7$, which was shifted to the Γ point by $0.05\Gamma X$ in order to align with the Fermi momentum of Sr_2RuO_4, is also shown in (c) (open circles).

which should be related with the observed kink. In a previous Raman study, the electron-phonon interaction for the apical oxygen vibration modes was discussed [40]. However, it is not clear for the zone-center apical oxygen phonon modes to couple with the Δ_4 band consisting of the out-of-plane Ru $4d_{yz,zx}$ orbitals, which shows the kink. In order to discuss the essential interpretation of the kink, the detailed study on the high-energy phonon modes and the possibility of the magnetic excitations as the origin of the layered ruthenates are strongly desired.

Finally, we discuss the influence of the orthorhombic distortion of $Sr_3Ru_2O_7$ on ARPES spectra. Figure 4(a) shows the MDC's spaced by 5 meV in an expanded momentum scale. MDC at E_F along the ΓX line and the expanded view are shown in Fig. 4(b). Two additional weak spectral features, denoted by A′ and B′ are clearly shown together with the prominent spectral features A, B, and C in the MDC spectra at E_F in Fig. 4(b). Those weak features disperse upward in energy with a decrease in the momentum, being opposite to that of the prominent ones. The MDC-derived dispersions due to the weak and prominent spectral features are shown by open and solid circles, respectively, in Fig. 4(c). The dispersions of the prominent spectral features A and B folded back along the $0.5\Gamma X$ line also are shown by the broken lines in Fig. 4(c). The dispersions of the weak bands are well consistent with that of the replica of the prominent bands. This means that the weak band features are simply caused by the reduction of the Brillouin zone due to the orthorhombic distortion. The distortion occurs in the bulk [41,42] and/or at the surface as reported in that for Sr_2RuO_4 [21]. Our ARPES spectra shows that the change in the electronic structure due to the distortion is not so large and that the prominent and the weak features are interpreted in terms of the electronic structure for the ideal tetragonal structure and the replica due to the um-

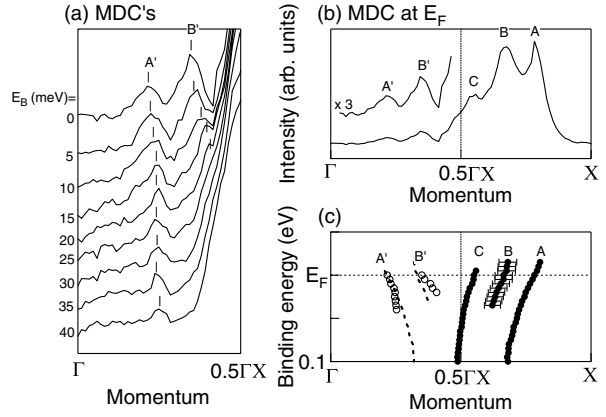

FIG. 4. (a) The same as in Fig. 2(a), but in an expanded momentum from the Γ point to the 0.5Γ*X* point. (b) MDC at E_F in the high symmetry line Γ*X* and the expanded view. (c) The MDC-derived dispersions (solid and open circles).

klapp bands, that is, weak Bragg diffraction by the orthorhombic distortion, respectively. This means that the orthorhombic distortion of $Sr_3Ru_2O_7$ does not affect the kink structure shown above.

We showed the kink in the dispersion of the monolayer and bilayer strontium ruthenates Sr_2RuO_4 and $Sr_3Ru_2O_7$, which is similar to the behavior of the kink for the cuprate superconductors [20]. Ruthenates have manifold Fermi surfaces derived from not only the in-plane Ru $4d_{xy}$ orbital but also out-of-plane Ru $4d_{yz,zx}$ orbitals, different from the cuprates which have a Fermi surface derived from only the in-plane Cu $3d_{x^2-y^2}$ orbital. Therefore, a further ARPES study for the multiband systems with complex Fermi surface topology, such as the RP-type ruthenates, may provide insight into the origin of the kink.

One of the authors (Y. A.) thanks H. Eisaki, T. Yoshida, and K. Tanaka for useful discussions. This work was partly supported by a Grant-in-Aid for COE Research (13CE2002) by the Ministry of Education, Science, and Culture of Japan. We thank the Cryogenic Center, Hiroshima University for supplying liquid helium. The synchrotron radiation experiments have been done under the approval of HSRC (Proposal No. 03-A-59).

*Electronic address: y.aiura@aist.go.jp

[1] Y. Maeno *et al.*, Nature (London) **372**, 532 (1994).
[2] K. Ishida *et al.*, Nature (London) **396**, 658 (1998).
[3] Y. Maeno, T. M. Rice, and M. Sigrist, Phys. Today **54**, No. 1, 42 (2001).
[4] A. Damascelli *et al.*, Phys. Rev. Lett. **85**, 5194 (2000).
[5] K. M. Shen *et al.*, Phys. Rev. B **64**, 180502 (2001).
[6] A. P. Mackenzie *et al.*, Phys. Rev. Lett. **76**, 3786 (1996).
[7] I. I. Mazin and D. J. Singh, Phys. Rev. Lett. **79**, 733 (1997).
[8] T. Kiyama *et al.*, J. Phys. Soc. Jpn. **67**, 307 (1998).
[9] T. Williams *et al.*, Mater. Res. Bull. **26**, 763 (1991).
[10] S. I. Ikeda *et al.*, Phys. Rev. B **62**, R6089 (2000).
[11] S. I. Ikeda *et al.*, J. Cryst. Growth **237**, 787 (2002).
[12] R. S. Perry *et al.*, Phys. Rev. Lett. **86**, 2661 (2001).
[13] S. A. Grigera *et al.*, Science **294**, 329 (2001).
[14] A. V. Puchkov, Z.-X. Shen, and G. Cao, Phys. Rev. B **58**, 6671 (1998).
[15] A. V. Puchkov *et al.*, Phys. Rev. Lett. **81**, 2747 (1998).
[16] I. Hase and Y. Nishihara, J. Phys. Soc. Jpn. **66**, 3517 (1997).
[17] D. J. Singh and I. I. Mazin, Phys. Rev. B **63**, 165101 (2001).
[18] Y. D. Chuang *et al.*, Phys. Rev. Lett. **87**, 117002 (2001).
[19] D. L. Feng *et al.*, Phys. Rev. Lett. **86**, 5550 (2001).
[20] X. J. Zhou *et al.*, Nature (London) **423**, 398 (2003).
[21] R. Matzdorf *et al.*, Science **289**, 746 (2000).
[22] K. Shimada *et al.*, Nucl. Instrum. Methods Phys. Res., Sect. A **467**, 504 (2001).
[23] K. Shimada *et al.*, Surf. Rev. Lett. **9**, 529 (2002).
[24] S. Hüfner, *Photoelectron Spectroscopy: Principles and Applications*, Springer Series in Solid-State Sciences Vol. 82 (Springer-Verlag, New York, 1995), Chap. 6.
[25] Y. Aiura *et al.*, Phys. Rev. Lett. **91**, 256404 (2003).
[26] T. Oguchi, Phys. Rev. B **51**, 1385 (1995).
[27] D. J. Singh, Phys. Rev. B **52**, 1358 (1995).
[28] I. Hase and Y. Nishihara, J. Phys. Soc. Jpn. **65**, 3957 (1996).
[29] Symmetry symbols are taken from the notation used in the band calculation for the same body centered tetragonal structure La_2CuO_4; K. Takegahara, H. Harima, and A. Yanase, Jpn. J. Appl. Phys. **26**, L352 (1987).
[30] Y. Yoshida *et al.*, J. Phys. Soc. Jpn. **67**, 1677 (1998).
[31] A. Lanzara *et al.*, Nature (London) **412**, 510 (2001).
[32] There is general agreement that the γ sheet is mainly derived from the in-plane Ru $4d_{xy}$ orbital and the α and β sheets from the out-of-plane Ru $4d_{yz,zx}$ ones. Along the high symmetry line Γ*X*, however, previous band calculations showed that the β sheet comes from the Δ_1 band due to the in-plane Ru $4d_{xy}$ orbital and the γ sheet from the Δ_4 band due to the out-of-plane Ru $4d_{yz,zx}$ ones [26–28].
[33] Y. Maeno *et al.*, J. Phys. Soc. Jpn. **66**, 1405 (1997).
[34] Z.-X. Shen *et al.*, Philos. Mag. B **82**, 1349 (2002).
[35] T. P. Devereaux, T. Cuk, Z. X. Shen, and N. Nagaosa, cond-mat/0403766 [Phys. Rev. Lett. (to be published)].
[36] H. He *et al.*, Phys. Rev. Lett. **86**, 1610 (2001).
[37] H. He *et al.*, Science **295**, 1045 (2002).
[38] J. Hwang, T. Timusk, and G. D. Gu, Nature (London) **427**, 714 (2004).
[39] M. Norman, Nature (London) **427**, 692 (2004).
[40] S. Sakita *et al.*, Phys. Rev. B **63**, 134520 (2001).
[41] Q. Huang *et al.*, Phys. Rev. B **58**, 8515 (1998).
[42] H. Shaked *et al.*, J. Solid State Chem. **154**, 361 (2000).